

## Relationships between Breakthrough Curves and X-ray Computed Tomography Analyzed Macropore Characteristics

Ten undisturbed soil monoliths of clayey Pelosol from Gottingen, Germany, covering the horizons A<sub>1</sub> and P<sub>1</sub> were collected. Some columns were left at natural humidity, some were oven-dried to simulate drought situations in forest soils in consequence of climate change. In seven columns, four micro-lysimeters, each, were installed at half the height in order to obtain data for analysis of single solute pathways. A fixed amount of KBr tracer was applied to the humus layer. The columns were irrigated with CaCl<sub>2</sub>. Column output and lysimeter output were collected and analyzed to record breakthrough curves. Bimodal analytical convection dispersion equation (CDE) solutions were fitted for the column outputs using a non-linear least square fit. A simple CDE solution did not fit well. This supports the model of two overlapping transport phenomena. After breakthrough recording was complete, all columns were scanned using X-ray computed tomography (CT). From the CT data 3-D reconstructions of the porous system were created for visual inspection, and the exact pathways for macropores along the micro-lysimeters were determined. Additionally, indices of the pore structure were computed to compare with the low and fast dispersivity values from the bimodal CDE fit. The variation in micro-lysimeter performance could be explained using the 3-D reconstruction. Statistically significant differences between the pore structure of wet and dried columns after the end of irrigation could not be identified. The pore index has generally a negative linear relationship with the fast dispersivity, and a positive linear relationship with the low dispersivity. These relations are stronger in the topsoil. The CT pictures and 3-D reconstructions provide an interesting insight into the soil pore system and may help to understand man-made drought problems due to climate change.

**Keywords:** Tracer transport, X-ray computed tomography, 3-D visualization, bimodality, CDE, dispersivity, BTC/breakthrough curves

The main research question of this work was to find out, if single pathways in unsaturated flow of wet and dried soils (with regard to droughts due to climate change) could be characterized in their functions. Quantitative relationships between soil structure (especially macropore characteristics, namely their size, number, type, distribution and continuity) and soil hydraulic properties are essential for improving our ability to model flow and transport in structured soils. Bouma (1979) and others have used chloride breakthrough curves from undisturbed soil columns

as an indirect means of characterizing macropores. In recent years, X-ray computed tomography (CT) data, which is based on varied linear attenuation of water, air and solid materials, provided an attractive tool for soil scientists to non-invasively observe soil structure (Gantzer and Anderson 2002; Luo *et al.* 2008; Taina *et al.* 2008; Kumar *et al.* 2010). Warner *et al.* (1989) used CT data to investigate the macropore system, e.g. characterization of cracks, earthworm holes and rooting channels. Peyton *et al.* (1992) concentrated on macropores, quantifying macropore perimeters, the paths surrounding macropore shapes. A relationship between macropores visualized by CT data and preferential flow was investigated by Heijss *et al.* (1996). Luo *et al.* (2010) related macropore characteristics quantitatively to solute transport parameters under saturated conditions. Borges and Pires (2012) have studied the representative

**Comment [D1]:** Germani,

**Comment [D2]:** P,

**Comment [D3]:** Humidity, and

**Comment [D4]:** For the analysis

**Comment [D5]:** Analyzed

**Comment [D6]:** squares

**Comment [D7]:** index generally has

**Comment [D8]:** reconstructions

**Comment [D9]:** in the unsaturated

**Comment [D12]:** air, and

**Comment [D10]:** distribution,

**Comment [D13]:** e.g., the

**Comment [D14]:** holes, and

**Comment [D11]:** columns,

**Comment [D15]:** paths

**Table 1.** Description of experimental design

Column number	Treatment (type)	Water content (%) (mean)	Br-Pulse <sub>0</sub> [day] (Bramount [mg])	Recovery rate (%)
1-4	Natural humidity (1)	37.5	0.833 (14.9-16.4)	76.9-85.9
5-7	Oven-dried (2)	30.7	0.833 (15.8-18.3)	55.2-91.1
10-12	Oven-dried (3)	30.7	0.0833 (15.3-17.3)	46.6-68.0

**Comment [D16]:** of the experimental

**Comment [D17]:** Water

elementary area (REA) of soil samples using CT data, and concluded that samples with volumes from 50 cm<sup>3</sup> to 100 cm<sup>3</sup> with minimum cross section of 640 mm<sup>2</sup> are enough to be representative for the soil structure. Our soil samples had volumes of about 5000 cm<sup>3</sup> with a cross section of 169 cm<sup>2</sup>.

The present study was carried out at University of Göttingen, Institute for Soil Science and Forest Nutrition, Büsgenweg, Germany on soil columns of a clayey Pelosol (Vertic Cambisol) with well described well-shrink characteristics (Spangenberg *et al.* 2011).

The objectives were to study the role of pore contact of micro-lysimeters in the soil column on tracer transport in relation to the structure, as assessed by X-ray CT under different initial conditions and irrigation. As it is not possible to carry out these investigations under field conditions, non-destructive CT data were used, making it possible for 3-D reconstruction of the structure of the investigated soil columns. Furthermore, using CT data, an attempt was made to understand the relationship between the breakthrough curves of the tracers (velocity, dispersion and dispersivity) and the measured volume and structure of the pores.

## Materials and Methods

### The soil studied

The soil in the present study is a clayey Pelosol (Vertic Cambisol), developed from a Muschelkalk (shell-lime) plateau derived from Triassic sediment layers. Collected horizons were O<sub>10</sub>-A<sub>n</sub>-P, O<sub>10</sub> was removed, only A<sub>n</sub> remained. The Ph horizon showed a polyedric structure (loamy clay). In this horizon, swell-shrink characteristics are well expressed, and swelling clay minerals accounted for 26 ± 5%. Mineral composition shows quartz, illite, corrensite, orthoclase, albite and goethite. The details of the soils and the experimental setup were given in Spangenberg *et al.* (2011). A representative sample was taken in the area where the soil columns were

taken. This sample was analyzed for soil density in various depths. Bulk density ranged from 0.908 Mg m<sup>-3</sup> (topsoil, A<sub>n</sub>) to 1.569 Mg m<sup>-3</sup> (subsoil, P, 20-30 cm depth).

### The column experiment

Originally, twelve undisturbed soil columns were collected in plexiglass cylinders of 14.7 cm diameter and about 30 cm height from a 4 m<sup>2</sup> sampling area. Ten columns were selected for this study, but in order to reduce the total amount of figures only columns 1, 5 and 12 are represented and described in detail. Table 1 shows an overview of the experimental design. Four columns (1-4) were kept at their natural mean water content of about 37.5% (mean value, n=4). Columns 5-7 and 10-12 were dried at 105 °C in a heating cabinet to a water content of 30.7% (Table 1). Four micro-lysimeters, each, were installed in seven soil columns. These micro-lysimeters were equipped with a hydrophilic porous polymertube (diameter 2.3 mm), made by Eijkkelkamp Agrisearch Equipment, Netherlands (Spangenberg *et al.* 1997).

They were designed specifically to minimize the impact of installation in soil. They were installed at about half the height of the column in order to allow observation of the flow parameters in higher temporal and spatial resolution in addition to the bottom output.

All columns were irrigated in a vacuum packed plexiglas container, which is a complete soil microcosm (described in Spangenberg *et al.* 2011).

Irrigation was applied using an electronic device every 2 h. At the bottom of each monolith, unsaturated flow was adjusted to 300 hPa. A bromide pulse was applied to each column at the beginning of the experiment. Then regular irrigation with CaCl<sub>2</sub> was started, which lasted for at least 30 days, *i.e.*, until no more bromide was found in the column output. Solution samples were collected daily at the bottom and from the micro-lysimeters of each column. They were analyzed for chloride and bromide. Analyses were done by HPLC ion chromatography. Elution mixture contained

**Comment [D18]:** Volumes ranging

**Comment [D26]:** Mg.m<sup>-3</sup>

**Comment [D19]:** With a minimum

**Comment [D20]:** of

**Comment [D21]:** at the university

**Comment [D22]:** Germany,

**Comment [D27]:** Total number of figures

**Comment [D28]:** 1, 5, and

**Comment [D29]:** On the soil

**Comment [D23]:** Dispersion, and

**Comment [D30]:**

**Comment [D31]:** hours.

**Comment [D24]:** Removed, and only

**Comment [D32]:** *i.e.*, until

**Comment [D25]:** Albite,

**Comment [D33]:** The elution

Na<sub>2</sub>CO<sub>3</sub> (2mmol) and NaHCO<sub>3</sub> (0.75mmol).  
 Detection limit of both elements was 300 μg L<sup>-1</sup>. The statistical analysis was done using SAS (Statistical Analysis System, SAS Institute, Inc., Cary). The procedure "nlin" of SAS was used to provide least squares modeling. An analytical solution of the convection dispersion equation (CDE) was used to fit the breakthrough curves of the experiment (van Genuchten 1982). Model parameters were estimated using bimodality, since it resulted in the best fit (Spangenberg *et al.* 2011).

### BTC Modeling

The most important models for solute transport in soil describe concentration changes in time and space using the CDE according to Nielsen and Biggar (1962).

$$R \frac{\partial C}{\partial t} = D \frac{\partial^2 C}{\partial x^2} - v \frac{\partial C}{\partial x} \quad \dots (1)$$

where, C = concentration [ML<sup>-3</sup>]; t = time [days]; x = spatial distance [L]; D = dispersion coefficient; v = average pore velocity [LT<sup>-1</sup>]

$$R = \text{Retardation (dimensionless)} \quad R = 1 + \frac{\rho_b K_d}{\theta} \quad \dots (2)$$

where,

ρ<sub>b</sub> = soil density [ML<sup>-3</sup>]; K<sub>d</sub> = constant factor [L<sup>3</sup>M<sup>-1</sup>]; ρ = volumetric water content [L<sup>3</sup>L<sup>-3</sup>]

According to Toride *et al.* (1995) R can be set on 1.

Starting (1.0) and boundary conditions (1.1 and 1.2) are:

$$C(x, 0) = C_i \quad \dots (1.0)$$

$$\left( -D \frac{\partial C}{\partial x} + v \right)_{x=0} = \begin{cases} v C_0 & 0 < t \leq t_0 \\ 0 & t > t_0 \end{cases} \quad \dots (1.1)$$

$$\frac{\partial C}{\partial x}(\infty, t) = 0 \quad \dots (1.2)$$

Assuming altered infiltration and disturbed water flow due to soil drought, the conditions for application of the CDE on treatment type 2 and 3 (Table 1) were incomplete. But concentrating on the aim of the investigation - a comparison between different experimental variants of dried and humid soils - the same methods of data analysis had to be chosen. To consider different flow behavior of dried and non-dried soils, new boundary conditions for the use of an analytical solution of the CDE were involved (Nielsen and Biggar 1962). A bimodal variant of this CDE was used, more details on this part are provided in Spangenberg *et al.* (2011).

### X-ray computed tomography

After the irrigation phase, the columns with installed micro-lysimeters were tomographed in a Hospital of Goettingen University. A medical CT scanner (HiSpeed Advantage, General Electric) was used. For the purpose of four 30 cm long soil columns, the head-neck settings were chosen. To understand the differences between moist and dry treatments, each soil column was tomographed individually. The output of the CT unit is in Hounsfield Units (HU), which is an internationally standardized numbering scale (Petrovic *et al.* 1982). The numerical value of Hounsfield Unit depends on the attenuation coefficients of the subject matter relative to that of water (Hainsworth 1983; Grever *et al.* 1989; Heijset al. 1995), which is given as  $H = 1000(\mu - \mu_w) / (\mu_w - \mu_a)$ . Here, μ is the linear attenuation coefficient of the material or pixel in question, μ<sub>w</sub> and μ<sub>a</sub> are the attenuation coefficients of water and air, respectively. A 512 by 512 matrix of pixel data was obtained for each scan. A pixel had the width of about 0.76 mm. This scan was taken at intervals of 2 mm (ca. 140 scans per column). A constant 1000 was added to every value, which is used on all CT scanners, and given in formula for H. After this addition, air has a value of 0 and water 1000. For each pixel, the X-ray attenuation values were stored as values from 0 to 4095. This range was due to the 12-bit processing of the tomography equipment. The high values correspond to the metal of the micro-lysimeter. The PV-WAVE was used for computer analysis, which allowed reconstructing, visualizing and quantifying 3-D macro pore structure in the soil column (Pierret *et al.* 2002).

### Indicators for pore structure

The most important outcome of the CT data is the information on the content of solids and soil porosity. The 12-bit data was reduced to 8-bit data and the whole dataset was scaled by dividing all the values by a factor 16, so that we have values ranging from 0-255. Good spatial resolution can be achieved when there is a large difference in H values between a subject (e.g., soil pore) and the background (e.g., soil matrix) as suggested by Grever *et al.* (1989).

In the present study, the same interior region of the top- and subsoil in all the soil columns was selected, the area around the micro-lysimeter was intentionally left out. These selected interior regions were divided into roughly cubic areas. These cubes form the basis for further data processing. Ideal cubes

Comment [D34]: The detection

Comment [D43]: hospital at

Comment [D35]: Modelling

Comment [D44]: question, and

Comment [D45]: had a width

Comment [D46]: (ca. 140

Comment [D47]: In the formula

Comment [D36]: (1995), R

Comment [D37]: To 1.

Comment [D48]: Data,

Comment [D38]: Drought,

Comment [D39]: Types 2

Comment [D49]: Factor of 16

Comment [D50]: e.g.,

Comment [D51]: (e.g., a soil matrix),

Comment [D40]: Consider the different

Comment [D41]: behaviors

Comment [D42]: soil,

Comment [D52]: Top and

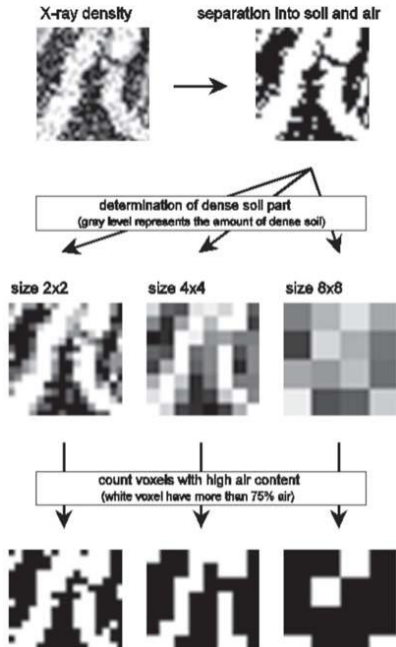


Fig. 1. Step-wise calculation for three cube sizes. (distribution of X-ray attenuation values, separation of soil solids and air; determination of soil solids (gray areas show the extent of soil solids); cube size  $2 \times 2$ ,  $4 \times 4$ ,  $8 \times 8$  counting of cubes with high air volumes (white cubes have more than 75% air volume))

are not possible with the given voxel size. Therefore, different sizes were reconsidered, namely,  $[4, 4, 1]$  voxel (labeled  $2 \times 2$ ),  $[8, 8, 2]$  voxel (labeled  $4 \times 4$ ) and  $[16, 16, 4]$  voxel (labeled  $8 \times 8$ ). These cubes correspond to volumes from  $1.8 \text{ mm}^3$  to about  $1 \text{ cm}^3$ . The step-wise calculation for the 3 cubes is presented in figure 1.

First, a threshold was selected to distinguish between dense matter and pores. A value of 110 was selected, as this provided the best separation based on known material locations. The percentage of cubes with less than 25% dense soil was computed for each sample area and cube size, which are labeled  $P_1$ ,  $P_2$ , and  $P_3$ , depending on cube size. These were used as indexes for the pore structure of a column. For a completely homogeneous material, all indexes would be the same. We used  $P_1$  as an index for the fine pore structure and  $P_3$  as an index for the coarse pore structure. The indexes do not represent the connectivity of porous volume, only the amount of

pores at a specific scale. The dispersivity values from bimodal tracer description were related to these indices for pore structure at three different scales. These indices were compared to the dispersivity results of the CDE models.

### 3- Reconstruction of soil structure

In the core of the column, which has a cross-sectional area of about  $10 \text{ cm} \times 10 \text{ cm}$ , the voxels with scaled attenuation values from 0 to 30 were reconstructed as a 3-D image of soil structure. This allows a visual inspection of pore connectivity for qualitative analysis. A value of 30 was chosen to allow the air-filled inner parts of macropores to be visible. For a better view of the pore contact of each lysimeter, the slice with the lysimeter was reconstructed separately in three viewing angles ( $40^\circ$ ,  $70^\circ$  and  $85^\circ$ ) with same viewing angle in all cases, i.e. for all columns (Figs. 2, 3 and 4). However, only slice with  $40^\circ$  viewing angle was presented. In order to overcome the effect of air pockets in the outer space around the soil column, the central square area of  $10 \text{ cm} \times 10 \text{ cm}$  was selected for the 3-dimensional reconstruction. At the top as well as at the bottom, some slices of the column were discarded. The location of the micro-lysimeters in the column were established, in which the x-, y- and z-coordinates of the lysimeter head and terminal in the cross-section image were determined.

### Results and Discussion

#### Influence of placement of micro-lysimeters and their function

The suction lysimeters of the tracer experiment drain different quantities of solution, although during the entire conduct of the experiment, a suction of  $0.030 \text{ MPa}$  was maintained. The great variability in the quantity of drained solution appears to be caused by the difference in positioning of the micro-lysimeters in the columns, relative to the porous system of the column. Preferential flow may initially have bypassed the lysimeters altogether, but relative position to the porous system seem to have a high influence. In order to explain this phenomenon, one column in each group is presented in figures 5, 6 and 7. Each figure contains a cross-section image at the height of the micro-lysimeters, a schematic of micro-lysimeter placement and the daily amounts of solution drained. The figures are used to judge the relative suction performance of the lysimeters. All four lysimeters of column 1 shows similar performance (Fig.

Comment [D53]: From the

Comment [D64]: at three

Comment [D65]:  $70^\circ$ ,

Comment [D66]: With the same

Comment [D67]: i.e.,

Comment [D68]: 2, 3,

Comment [D69]: only a slice

Comment [D70]: with a  $40^\circ$ -degree

Comment [D71]: a central square

Comment [D72]: bottom,

Comment [D73]: was established,

Comment [D74]: and

Comment [D54]: distribution

Comment [D55]: solid (gray areas

Comment [D56]: volum

Comment [D75]: of the placement

Comment [D57]: labelled

Comment [D58]: labelled  $4 \times 4$

Comment [D59]: volumes ranging from

Comment [D60]: First,

Comment [D76]: in the porous

Comment [D61]: labelled  $P_1$ ,  $P_2$ ,

Comment [D62]: on the cube

Comment [D63]: structure,

Comment [D77]: in column 1

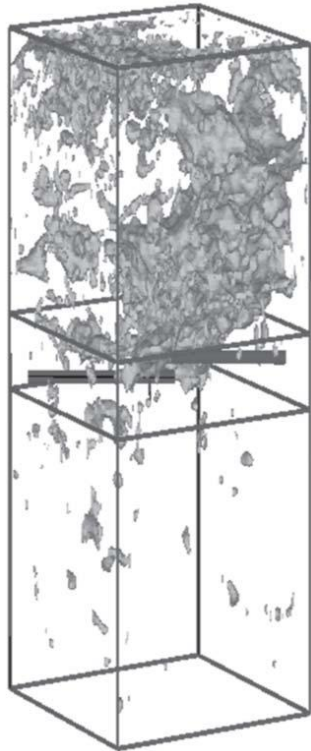


Fig.2a,Column1,withsection

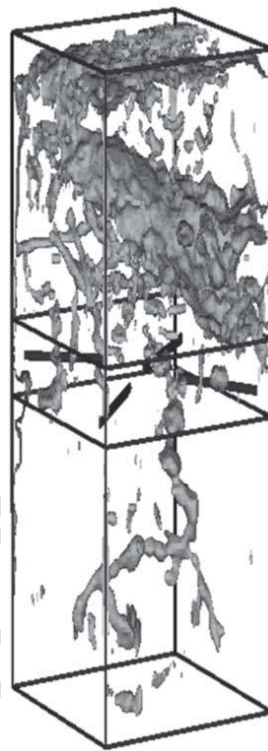


Fig.3a,Column5,withsection

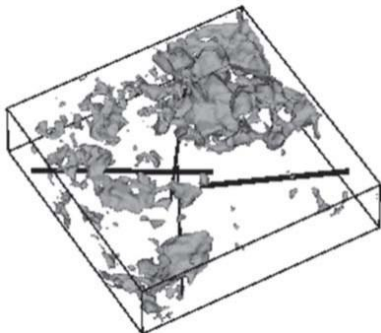


Fig.2b,Column1,section,40degree

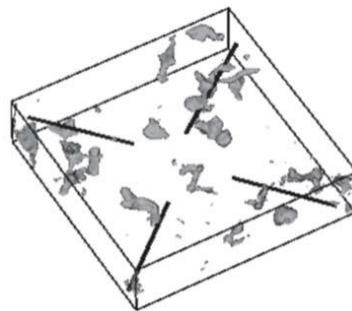


Fig.3b,Column5,section,40degree

**Fig.2.3-**Dreconstructionofcolumn1(experimentalvariant 1)withinstalledmicro-lysimeters.Inthecoreofthe column,thescaledattenuationvaluesfrom0to30are presented.Forabetterview,thissectionwiththelysimetersispresentedina40degreelook-angle.Thecore ofthecolumnhasacross-sectionalareaof10cm×10cm

**Fig.3.3-**Dreconstructionofcolumn5(experimentalvariant 2)withinstalledmicro-lysimeters.Inthecoreofthe column,thescaledattenuationvaluesfrom0to30are presented.Forabetterview,thissectionwiththelysimetersispresentedina40degreelook-angle.Thecore ofthecolumnhasacross-sectionalareaof10cm×10cm

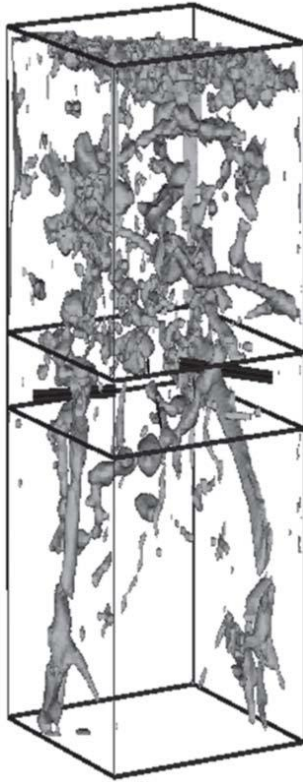


Fig.4a,Column12,withsection

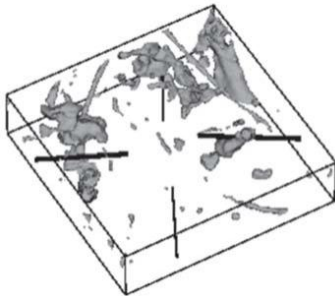


Fig.4b,Column12,section,40degree

Fig.4.3-Dreconstructionofcolumn12(experimentalvariant 3)withinstalledmicro-lysimeters.Inthecoreofthe columnthescaledattenuationvaluesfrom0to30are presented.Forabetterview,thesectionwiththelysimetersispresentedina40degreelook-angle.Thecore ofthecolumnhasacross-sectionalareaof10cm×10cm

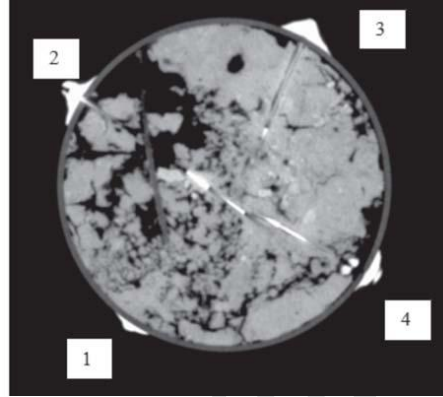


Figure5a,cross-sectionofcolumn1withmicro-lysimeters (topleft:no2;topright:no3;bottomleft:no1;bottomright: no4)andtheirnumbering

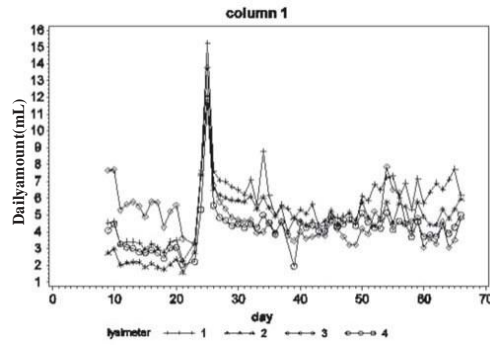


Fig.5bSamplevolumes(ml)ofcolumn1

Fig.5.Cross-sectionimageofcolumn1withmicro-lysimetersandtheirnumbering(5a)aswellasmicro-lysimeters' respective measured sample volumes (mL), column 1 (5b)

5c).Micro-lysimeters2and4showidenticalcurves, evenbeforeandafterthebreakincontinuityof leaching.Theirtipslieclosetoeachother(Fig.5a and5b),soweassume,thesesuctionlysimetersshowed reciprocalinfluence.Modelingofthe breakthroughcurvesdidn'tmake sense.Incolumns5 and12,bothpreviouslydried,atleastonemicro-lysimeterhad direct contact with a macropore (Fig.6a, micro-lysimeter no 4 and Fig.7 a micro-lysimeter no 15).Thesemicro-lysimeters showed the lowest suction performance within their column.Thus,contact to a macropore (>0.5cm) appears to have a clear influence on the suction performance of a micro-

Comment [D78]: in the continuity

Comment [D79]: The modelling

Comment [D80]: no. 4, and

Comment [D81]: 7a,

Comment [D82]: no. 15

Comment [D83]: with a macropore

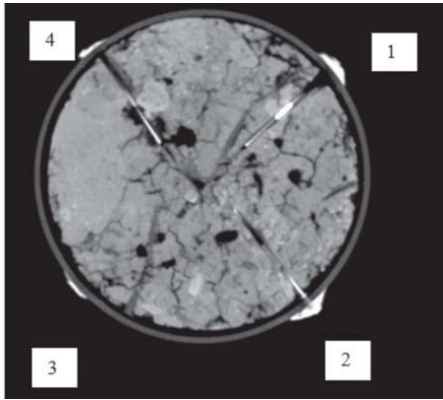


Fig. 6a Cross-section of column 5 with micro-lysimeters (top left: no 4; top right: no 1; bottom left: no 3; bottom right: no 2) and their numbering

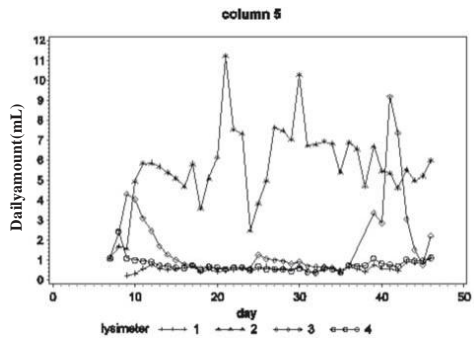


Fig. 6b Sample volumes (mL) of column 5

Fig. 6. Cross-section image of column 5 with micro-lysimeters and their numbering (6a) as well as micro-lysimeters' respective measured sample volumes (mL), column 5 (6b)

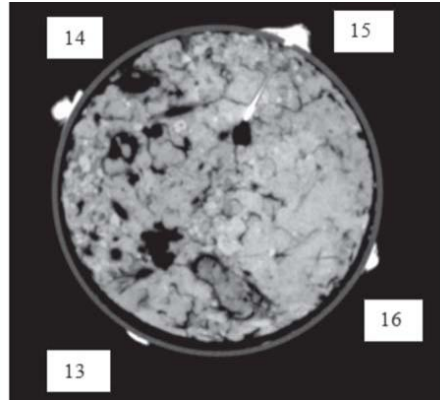


Fig. 7a Cross-section of column 12 with micro-lysimeters (top left: no 14; top right: no 15; bottom left: no 13; bottom right: no 16) and their numbering

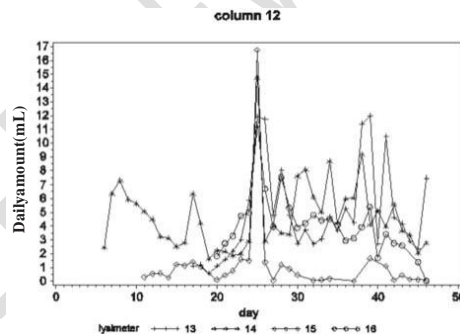


Fig. 7b Sample volumes (mL) of column 12

Fig. 7. Cross-section image of column 12 with micro-lysimeters and their numbering (7a) as well as micro-lysimeters' respective measured sample volumes (mL), column 12 (7b)

lysimeter. Under unsaturated conditions, only a thin film of water is present on the walls of pores of this diameter. Because of this, these suction lysimeters drained no solution most of the time, and hence low volume of leachate. Transferring this result to natural conditions where the micro-lysimeters would represent the rooting zone of forest trees, it can be assumed that already under these simulated drought conditions water stress would have begun.

Micro-lysimeters in a compact soil matrix also showed low suction performance. A placement avoiding these extremes resulted in satisfactory functioning. If enough fine pores are present in the vicinity of the micro-lysimeters, the capillary

contribution of water outweighs the air-filled porosity, and the volume of the leachate collected will be higher (Fig. 8). The median daily amount of leachate after the initial phase of the experiment is shown on the abscissa. On the ordinate, the content of the solids in the soil in an ellipsoidal region around the tip of the micro-lysimeter (ca. 12 cm<sup>3</sup>) is shown. Interestingly, the suction performance of the micro-lysimeter with high pore volume was as poor as for lysimeter with almost 100% compact soil around it (column 3). Most lysimeters show best performance with moderately compact soil. In addition to the total quantity of pores and soil volume, the pore size distribution and their connectivity to the immediate vicinity of the lysimeter

Comment [D87]: The contribution

Comment [D84]: resulting in a low

Comment [D85]: trees,

Comment [D86]: conditions,

Comment [D88]: them

Comment [D89]: in moderately

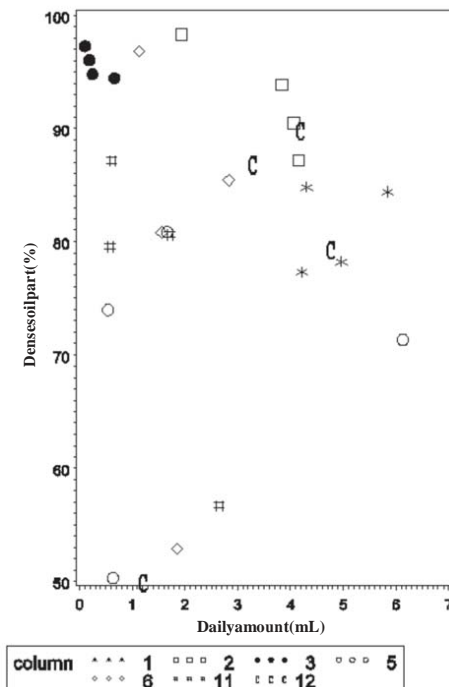


Fig.8. Percentages of soil solids around the lysimeter in relation to the suction performance of the lysimeter for 28 lysimeters in 7 columns. The soil solid content was obtained from the CT attenuation data

is important. All these factors appear to be responsible for the otherwise unexplained suction effectiveness of the lysimeters. Eight of the 28 lysimeters have to be considered to be ineffective, since they drain less than  $1 \text{ mL}^{-1}$  (Fig. 8). About 70% of the installed micro-lysimeters are capable of draining, and about half of them are distinctly useful ( $> 3 \text{ mL}^{-1}$ ) under the given conditions.

For the first time, CT analysis was able to visualize and reveal cause-effect relationships of micro-lysimeter pore contacts and their suction ability. The X-ray CT images of cross sections of the soil columns did not show noticeable disturbances in soil structure of the columns due to installation of the micro-lysimeters (Figs. 5a, 6a and 7a). In contrast to this, Beckmann *et al.* (1992) found noticeable disturbances in soil structure due to installation of standard lysimeter cups in the field, resulting in an alteration of the pore system. For most of the dried

columns (columns 5 and 12; Figs. 10 and 11) the micro-lysimeters have missed the main breakthrough as they had no initial soil contact because of the dry state of the soil, or the first fast breakthrough bypassed them.

*Localization of the micro-lysimeters and its relation to tracer breakthrough curves*

Given that no CDE model could be fit for the micro-lysimeter data, its breakthrough curves in relation to pore structure can only be discussed in a qualitative way. As examples, the 3-Dreconstructions of columns 1, 5 and 12 with installed micro-lysimeters are represented in figures 2, 3 and 4, respectively.

The breakthrough curves of all micro-lysimeters are available as well as all 3-Dreconstructions of the scanned soil columns. The breakthroughs of the micro-lysimeters of column 1 (the wet variant of the experiment) along with the breakthrough of the whole column are represented (Fig. 9). In this column, the maximum values of the micro-lysimeter breakthrough curves were lower than the column output. Obviously, there it was a fast breakthrough, which bypassed the micro-lysimeters and as a low breakthrough that was seized by the lysimeter. This similarity of the micro-lysimeter breakthroughs is explained by the fact that all 4 micro-lysimeters lied close to and influenced each other (Figs. 2 and 5a). In columns 2 and 3 the micro-lysimeters, to a great extent, attain higher bromide values earlier than column outflow

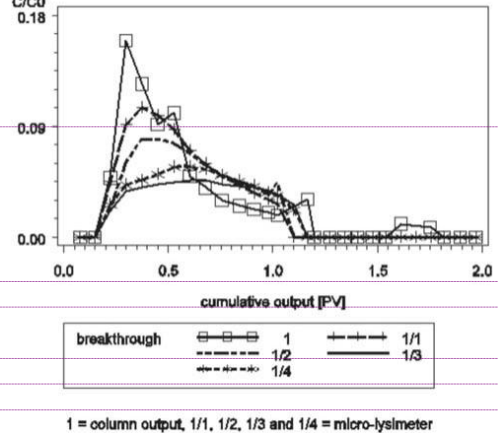


Fig.9. Breakthrough curves of column 1 (experimental variant 1) in units of the pore volume. C=measured concentration, C<sub>0</sub>=concentration of the Br pulses

Comment [D100]: their

Comment [D101]: examples,

Comment [D102]: 5,

Comment [D103]: 3,

Comment [D104]: available,

Comment [D105]: as are all

Comment [D106]: there was

Comment [D107]: through that bypassed

Comment [D90]: Percentage of soil

Comment [D91]: lysimeters

Comment [D92]: data.

Comment [D108]: outflow.

Comment [D93]: considered ineffective

Comment [D94]: cause-and-effect

Comment [D95]: between micro-lysimeter

Comment [D96]: in the soil

Comment [D97]: to the installation

Comment [D98]: 6a,

Comment [D99]: to the installation

Comment [D109]: concentration;

Comment [D110]: pulses.

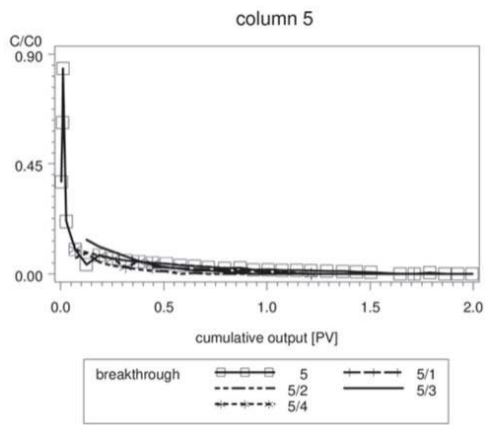


Fig.10. Breakthrough curves of column 5 (experimental variant 2) in units of the pore volume. C=measured concentration, C<sub>0</sub>=concentration of the Br-pulses

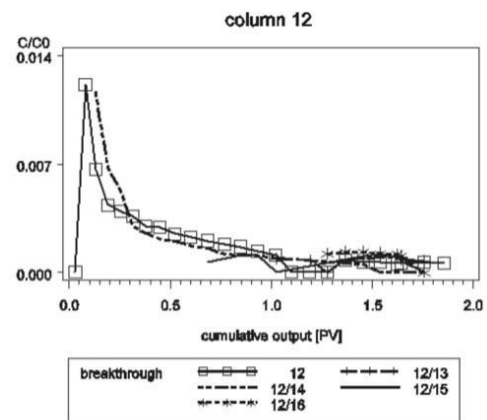


Fig.11. Breakthrough curves of column 12 (experimental variable 3) in units of the pore volume. C=measured concentrations, C<sub>0</sub>=concentration of the Br-pulses

(not shown). These lysimeters have participated in the fast breakthrough via the coarse pores, e.g. column 2 (not shown, lysimeters 5 and 7).

At least one micro-lysimeter of column 5 (Figs. 3, 6a and 10) had very clear contact to the middle of a coarse pore, which traversed through the soil column, and which possibly contributed to the fast transport. Because of the deficient initial soil contact or too low suction capacity, this lysimeter did not show the fast breakthrough. As single lysimeter of the

dry columns, lysimeter 14 of column 12 (Figs. 4, 7a and 11), showed an almost complete fast breakthrough. Of all the lysimeters of this column, this was the first to lead to soil solution leaching, and was present in the soil matrix with indirect contact to coarse pore space. This constellation, a mixing of indirect contact to coarse pore transport space and direct contact to the fine pore matrix, appear to have the best pre-condition for a quick functioning of the lysimeters, above all, in dried soil substance.

*Pore connectivity in the columns and their importance for tracer transport*

For a better understanding of the total transport through the columns, the transport in top soil and in subsoil was considered. These two were characterized by different soil structure and pore structure. The top soil had a more or less strongly expressed crumb structure with high porosity, whereas, the porosity in the subsoil was low, because of the clay content. Hence, its structure was strongly influenced by roots, faunal burrows, and shrinkage cracks through drying, therefore, contains macropores. Both soil regions, according to their expression of their main characteristics, differently influenced tracer transport in a column.

Lu *et al.* (2010) investigated quantitative relationships between macropore characteristics and two major flow and transport parameters ( $K_{sat}$  and  $\lambda$ ). Macropores played an important role. The traditional CDE modeled the BTCs well. Correlation between  $\lambda$  of the whole soil column and  $K_{sat}$  values of the B horizon (not A) implied that the dispersivity was mainly controlled by the horizon with the lowest  $K_{sat}$  in the soil column. The most useful macropore parameters for predicting flow and transport under saturated conditions in the structured soils included macroporosity, number of paths, hydraulic radius and macropore angle. The presence of traversing pores (not necessarily macropores in the classical sense) in the subsoil influence the velocity and concentration of the tracers transport in this part. The reconstruction of the flow pattern is difficult, although the parameters are early defined. This is because of the interplay of all factors, with initial and boundary conditions as water content can be different even in a small space but have a great influence. Further, the problem exists that only vertical transport mechanism was considered. As is known from dye-experiments, the horizontal transport also spread to a good extent (Ghodrati and Jury 1990), that is why, the vertically connected pores do not lead to preferential flow.

Comment [D111]: complete breakthrough.

Comment [D112]: lysimeters in this

Comment [D113]: contact with coarse

Comment [D114]: contact with the coarse

Comment [D115]: pore

Comment [D116]: contact with the fine

Comment [D117]: for the quick

Comment [D126]: importance

Comment [D127]: columns, transport

Comment [D128]: and subsoil

Comment [D118]: variable

Comment [D129]: drying; therefore, it

Comment [D130]: modelled

Comment [D131]: The correlation

Comment [D119]: concentrations

Comment [D132]: influences

Comment [D133]: tracer

Comment [D120]: e.g., column

Comment [D134]: including the

Comment [D135]: conditions,

Comment [D136]: because

Comment [D121]: 6a,

Comment [D122]: contact with the middle

Comment [D137]: mechanisms were

Comment [D123]: column and possibly

Comment [D138]: 1990). That

Comment [D124]: or the too

Comment [D125]: show a fast

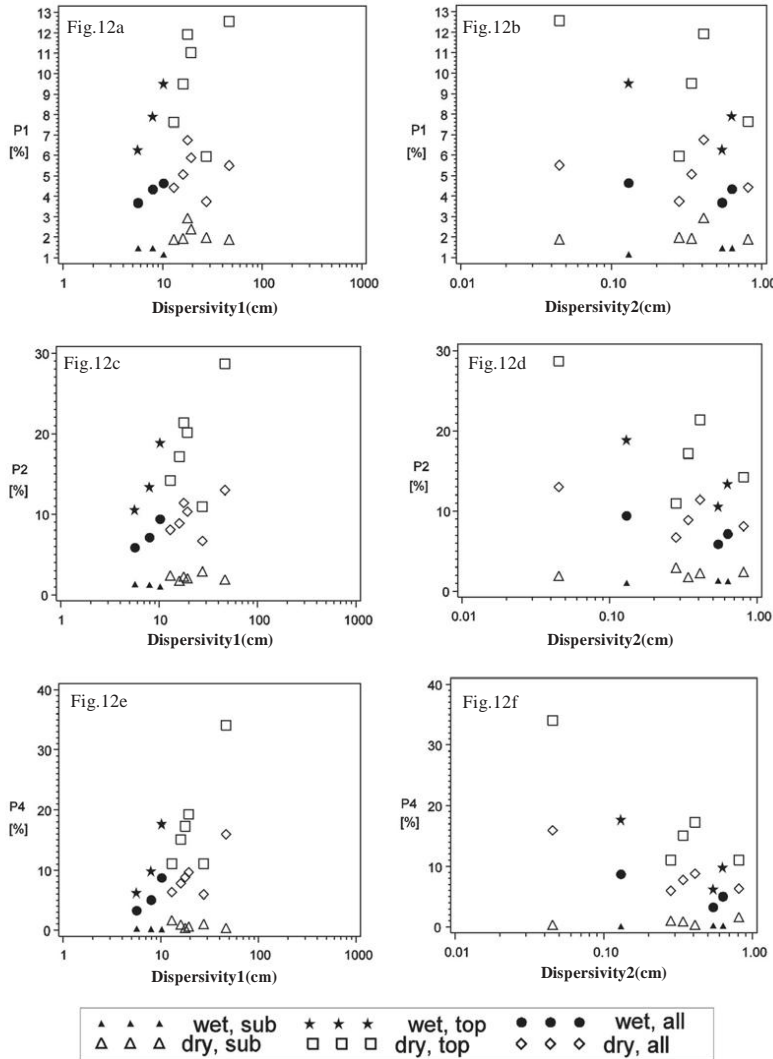


**Fig. 12.** Dispersivity of the bimodal approach in relation to pore structure at three different scales (P1, P2, P4); three values for the respective column. Dispersivity1 =  $D1/v1$  = fast breakthrough, dispersivity2 =  $D2/v2$  = slow breakthrough (Table 2). "Bottom" means subsoil of the column; "top" means topsoil and "comp." means complete column.

**Comment [D139]:** P2, and P4

**Comment [D140]:** topsoil;

**Comment [D142]:** integrated into water

**Comment [D141]:** soil took part

In the same way, Flury *et al.* (1994) reported that a major part of the water flowed past the soil matrix. As a result, an unexpectedly small portion of the soil, possibly took part in the transport. Boutilink and Bouma (1991) observed discontinuous macropores, so-called internal catchments, which

should be integrated in water flow modeling. From studies on soil structure using x-ray CT, it was reported by Luo *et al.* (2008) that no macropores were continuous from the top to the bottom of the soil column, and some macropores became ineffective because of air-entrapment. They concluded that

**Table 2.** Results of bimodal parameter evaluation. Retardation factor  $R=1$ , coefficient of dispersivity ( $\text{cm}^2 \text{Day}^{-1}$ ),  $v$ =average pore water velocity ( $\text{cm Day}^{-1}$ ),  $D/v$ =dispersivity (cm), Br=Bromide quantity of the impulses (mg).

Column	$D1/v1$ (cm)(cm)(mg)	$D2/v2$	Br
1	9.0	0.18	14.3
2	8.0	0.63	16.0
3	5.7	0.54	15.0
4	14.5	0.3	15.7
5	19.3	0.0	32.4
6	38.1	0.08	34.5
8	16.0	0.34	14.3
10	24.4	0.49	16.4
11	23.1	0.26	16.8
12	12.9	0.81	11.5

macropore network by itself cannot simply be equated to a preferential flow network. Accordingly, in the description of flow process, a series of complex processes need to be considered.

In order to describe the relationship between the BTC and the soil pore characteristics, we opposed fit parameters of the CDE and soil pore indices. As explained earlier, the indexes ( $P_1, P_2$  and  $P_4$ ) were computed for the pore structure of a column.  $P_1$  is an index for pore structure on a smaller scale. The  $P_4$  on the other hand, is an index for coarse pore structure (Fig. 1). The respective indexes,  $P_1, P_2$  and  $P_4$  are shown on the ordinate. On the abscissa, either the dispersivity of the slow ( $D_1/v_1$ ) or fast ( $D_2/v_2$ ) are shown (Fig. 12, Table 2). The symbol represents the variant of the experiment (dry, wet) and the area of the column the index applies to (top=top-soil, bottom=sub-soil, comp.=complete column).

In figures 12b, 12d and 12f, corresponding fast dispersivity values ( $D_2/v_2$ ) in relation to indexes for fine ( $P_1$ ), middle ( $P_2$ ), or coarse ( $P_4$ ) pores were presented. At all three scales these figures showed a negative relationship to dispersivity, which increased with decreasing air content. This relationship was stronger for coarse pore indexes in topsoil. The transport pathway appeared to be shortened by higher air content, which lowered fast dispersivity. When coarse pores were present in the columns ( $P_4$ ), then with fast breakthrough, uniform flow was to be expected, without heterogeneity of pathway of water and chemical movement. Nearly linearly decreasing lines could be observed (Fig. 12f) for topsoil and whole column indexes. This happened to a lesser extent even with more finely divided pore space

(Fig. 12d). The low dispersivity values had a positive relationship to the pore indices for all scales (Fig. 12a, 12c and 12e) and soil areas, which was nearly linear in all scales. With growing pore content the heterogeneity of the pathways increased. Again, this relationship was more apparent in topsoil.

All results have to be considered with a bit of caution, as the CDE fit was using a model, which for the dry column might be questionable. As a mathematical model it reached plausible dispersivity values, though. It explains why we could not detect differences among the soil columns just by visualizing. It can be assumed that all columns showed macropore transport, which was not linked to dispersivity of the sub-soils.

### Conclusions

The 3D reconstruction of the porous system can be used to discuss the suction performance of individual micro-lysimeters and for explaining the breakthrough curves of micro-lysimeters. A numeric pore index representing a volume's pore content at a specific scale can be computed from CT data, and does have a relation to flow parameters. The pore index has generally a negative linear relationship with the fast dispersivity, and a positive linear relationship with the low dispersivity. These relations suggest that with increasing porosity, the heterogeneity of the pathways increases. We conclude that the CT images like cross-sections and 3D reconstructions provide an interesting and quite unique insight into the soil pore system after moderate drying. Cross-sections visualizing the pore contact of micro-lysimeters' tips may help to interpret soil water monitoring in a better way.

### References

- Beckmann, T., Kücke, M., Hasenpusch, K. and Altemüller, H.J. (1992) Einbaubedingte Gefügeänderungen in der Bodenzone um keramische Saugkerzen. *Zeitschrift für Pflanzenernährung und Bodenkunde* **155**, 247-250.
- Booltink, H. W. G. and Bouma, J. (1991) Physical and morphological characterization of by-pass flow in a well-structured clay soil. *Soil Science Society of America Journal* **55**, 1249-1254.

Comment [D151]: In the topsoil

Comment [D152]: to the dispersivity

Comment [D153]: subsoils.

Comment [D154]: to explain

Comment [D143]: of the flow

Comment [D144]: opposed the fit

Comment [D155]: relationship

Comment [D145]: on a smaller

Comment [D156]: reconstructions,

Comment [D146]: is shown

Comment [D147]: At all three

Comment [D148]: appeared

Comment [D149]: of the pathway

Comment [D150]: space.

- Bouma, J. and Wosten, J. H. M. (1979) Flow patterns during extended unsaturated flow in two, undisturbed swelling clay soil with different microstructures. *Soil Science Society of America Journal* **43**, 16-22.
- Borges, J. A. R. and Pires, L. F. (2012) Representative elementary areas in soil bulk density measurements through gamma ray computed tomography. *Soil and Tillage Research* **123**, 43-49.
- Flury, M., Fluehler, H., Jury, W. A. and Leuenberger, J. (1994) Susceptibility of soil to preferential flow of water: A field study. *Water Resources Research* **30**, 1945-1954.
- Gantzer, C. J. and Anderson, S. H. (2002) Computed tomographic measurement of macroporosity in chisel-disk and non-tillage seedbeds. *Soil and Tillage Research* **64**, 101-111.
- Ghodrati, M. and Jury, W. A. (1990) A field study using dyestocharacterize preferential flow of water. *Soil Science Society of America Journal* **54**, 1558-1563.
- Grevers, M. C. J., De Jong, E. and Arnaud, R. J. St. (1989) The characterization of soil macroporosity with CT scanning. *Canadian Journal of Soil Science* **69**, 629-6.
- Hainsworth, J. M. and Aylmore, L. A. G. (1983) The use of computer-assisted tomography to determine spatial distribution of soil water content. *Australian Journal of Soil Research* **21**, 435-443.
- Heijs, A. W. J., Lange, J., de Schoute, J. F. and Bouma, J. (1995) Computed tomography as a tool for non-destructive analysis of flow patterns in macroporous clays. *Geoderma* **64**, 183-196.
- Heijs, A. W. J., Ritsema, C. J. and Dekkar, L. W. (1996) Three dimensional visualization of preferential flow pattern in two soils. *Geoderma* **70**, 101-116.
- Kumar, S., Anderson, S. H. and Udawatta, R. P. (2010) Agroforestry and grass buffer influence on macropores measured by computed tomography under grazed pasture systems. *Soil Science Society of America Journal* **74**, 203-212.
- Luo, L. F., Lin, H. S. and Halleck, P. (2008) Quantifying soil structure and preferential flow in intact soil using X-ray computed tomography. *Soil Science Society of America Journal* **72**, 1058-1069.
- Luo, L. F., Lin, H. S. and Schmidt, J. (2010) Quantitative relationship between soil macropore characteristics and preferential flow and transport. *Soil Science Society of America Journal* **74**, 1929-1937.
- Nielsen, D. R. and Biggar, J. W. (1962) Miscible displacement. 3. Theoretical considerations. *Soil Science Society of America Proceedings* **26**, 216-221.
- Peyton, R. L., Haeffner, B. A., Anderson, S. H. and Gantzer, C. J. (1992) Applying X-ray CT to measure macropore diameters in undisturbed soil cores. *Geoderma* **53**, 329-340.
- Petrovic, A. M., Siebert, J. E. and Rieke, P. E. (1982) Soil bulk density analysis in three dimensions by computer tomographic scanning. *Soil Science Society of America Journal* **46**, 445-450.
- Pierret, A., Capowiez, Y., Belzunces, L. and Moran, C. J. (2002) 3D reconstruction and quantification of macropores using X-ray computed tomography and image analysis. *Geoderma* **106**, 247-271.
- Spangenberg, A., Cecchini, G. and Lamersdorf, N. (1997) Analysing the performance of microsoils solutions sampling device in a laboratory examination and a field experiment. *Plant and Soil* **196**, 59-70.
- Spangenberg, A., Nagarajao, Y. and Hinz, Ch. (2011) Description of tracer transport through moist and dried soil columns using a bimodal CDE approach. *Fresenius Environmental Bulletin* **20**, 616-622.
- Taina, L. A., Heck, R. J. and Elliot, T. R. (2008) Application of X-ray computed tomography to soil science: A literature review. *Canadian Journal of Soil Science* **88**, 1-20.
- Toride, N., Leij, F. J. and van Genuchten, M. Th. (1995) The CXTFIT code for estimating transport parameters from laboratory or field tracer experiments. U.S. Salinity Laboratory, U.S. Department of Agriculture, Riverside, California Research Report, 137.
- van Genuchten, M. Th. and Alves, J. W. (1982) Analytical solutions of the one-dimensional convective-dispersive solute transport equation. *US Department of Agriculture Technical Bulletin*, 133-192.
- Warner, J. S., Nieber, J. L., Moore, I. D. and Geese, R. A. (1989) Characterizing macropores in soil by computed tomography. *Soil Science Society of America Journal* **53**, 653-660.